Perfusion-Based Functional Magnetic Resonance Imaging

AFONSO C. SILVA,[1] SEONG-GI KIM[2]

[1] *Laboratory of Functional and Molecular Imaging, National Institute of Neurological Disorders and Stroke,* 10 *Center Drive, Building* 10, *Room B1D*118, *Bethesda, Maryland* 20892-1065
[2] *Department of Neurobiology, University of Pittsburgh, Pittsburgh, Pennsylvania* 15261

ABSTRACT: The measurement of cerebral blood flow (CBF) is a very important way of assessing tissue viability, metabolism, and function. CBF can be measured noninvasively with magnetic resonance imaging (MRI) by using arterial water as a perfusion tracer. Because of the tight coupling between neural activity and CBF, functional MRI (fMRI) techniques are having a large impact in defining regions of the brain that are activated due to specific stimuli. Among the different fMRI techniques, CBF-based fMRI has the advantages of being specific to tissue signal change, a critical feature for quantitative measurements within and across subjects, and for high-resolution functional mapping. Unlike the conventional blood oxygenation level dependent (BOLD) technique, the CBF change is an excellent index of the magnitude of neural activity change. Thus, CBF-based fMRI is the tool of choice for longitudinal functional imaging studies. A review of the principles and theoretical backgrounds of both continuous and pulsed arterial spin labeling methods for measuring CBF is presented, and a general overview of their current applications in the field of functional brain mapping is provided. In particular, examples of the use of CBF-based fMRI to investigate the fundamental hemodynamic responses induced by neural activity and to determine the signal source of the most commonly used BOLD functional imaging are reviewed. Concepts Magn Reson Part A 16A: 16–27, 2003*

KEY WORDS: arterial spin labeling; brain; cerebral blood flow; magnetic resonance imaging

INTRODUCTION

Measuring cerebral blood flow (CBF) is a very important method to assess tissue viability, metabolism, and function. CBF can be measured noninvasively with magnetic resonance imaging (MRI) by using arterial water as a perfusion tracer (*1–8*). The general principle behind arterial spin labeling (ASL) techniques is to differentiate the net magnetization of endogenous arterial water flowing proximally to the organ of interest from the net magnetization of tissue. As arterial blood perfuses the tissue, water exchange occurs, effectively changing the net magnetization of tissue proportionally to the blood flow rate. Therefore, CBF can be quantitatively related to the difference of two images acquired consecutively: one with spin labeling and another as a control. ASL MRI techniques can be implemented with either pulsed labeling

Received 19 September 2002; accepted 1 October 2002

Correspondence to: Dr. A.C. Silva; E-mail: silvaa@ninds.nih.gov.
Contract grant sponsor: National Institutes of Health.
Contract grant number: RR08079.
Contract grant sponsor: University of Minnesota.
Contract grant number: NS38295.

Concepts in Magnetic Resonance Part A, Vol. 16A(1) 16–27 (2003)

Published online in Wiley InterScience (www.interscience.wiley.com). DOI 10.1002/cmr.a.10050

(*3–5, 7*) or continuous labeling (*2, 6, 8*). The pulsed ASL (PASL) methods use single or multiple RF pulses to label arterial blood water spins. The continuous ASL (CASL) technique (*2*) uses a long RF pulse in the presence of a longitudinal field gradient to label the arterial spins according to the principles of adiabatic fast passage (*9*). ASL techniques have major advantages over other techniques based on the administration of exogenous tracers. It is a completely noninvasive technique for measuring CBF. Further, because of the very short half-life of the labeled spins, repeated measurements of CBF can be performed as often as desired. Moreover, the techniques preserve the high spatial resolution of ^{1}H MRI, enabling a direct and precise anatomical localization of CBF changes. On the other hand, proper perfusion contrast is only achieved when enough time is allowed for the labeled arterial spins to travel into the region of interest and exchange with tissue spins. This makes it difficult to detect changes in CBF with a temporal resolution greater than the decay time of the label.

Due to the tight coupling between neural activity and CBF (*10*), the basis for modern functional neuroimaging methods (*11*), functional MRI (fMRI) techniques based on either changes in blood oxygenation level dependency (BOLD) (*12–14*), regional CBF (rCBF) (*5, 15*), or regional cerebral blood volume (rCBV) (*16*), are having a large impact in defining regions of the brain that are activated because of specific stimuli. With the continued improvement of MRI hardware, the spatial and temporal resolutions of fMRI have both improved. Higher spatial resolution means better spatial localization of fMRI signal changes. Better temporal resolution also means better spatial localization, as early hemodynamic events are likely to occur close to the site of increased neuronal activity. Nevertheless, the spatiotemporal relationship between hemodynamic changes probed by functional neuroimaging techniques and electrical neuronal events is still poorly understood and needs to be better characterized.

In particular, the BOLD contrast mechanism can be modeled as a complex interplay between relative CBF, CBV, and oxygen consumption changes ($CMRO_2$) (*17, 18*). However, the relationship between these variables is not fully understood. Positive BOLD signal changes are presumably caused by fractional increases in CBF that are unmatched by fractional increases in $CMRO_2$ (*17, 19*). This mismatch between CBF and $CMRO_2$ changes may not be present in all activated regions at all times (*20*). Furthermore, there is no clear model to quantify the changes in CBF from the measured BOLD signal changes. Therefore, to date, BOLD remains a qualitative technique. On the other hand, perfusion-based fMRI provides absolute quantification of CBF and provides potentially better spatial localization than BOLD because it is sensitive to the arterial side of the vascular tree, in particular to capillaries.

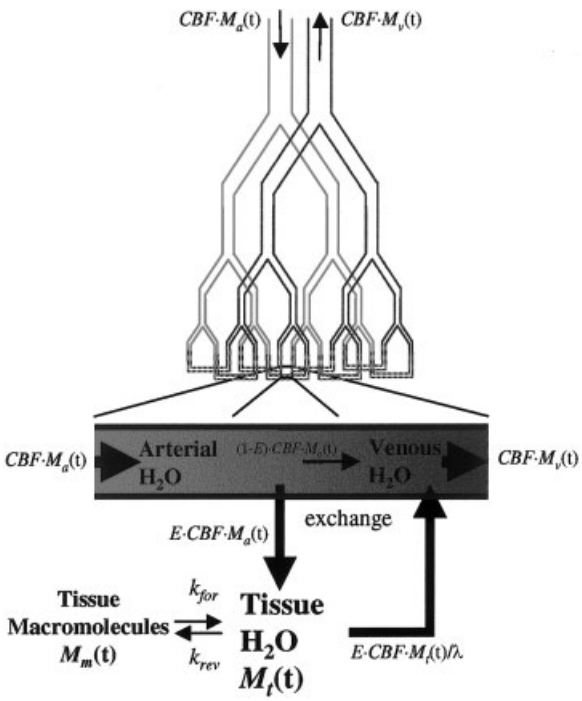

Figure 1 A schematic representation of an MR image voxel for the purposes of establishing the arterial spin labeling model. Blood flowing through the arterial vessels with flow rate CBF (mL g^{-1} min^{-1}) reach the capillary bed, where a fraction E of water exchanges with tissue water in the extravascular space. The remaining fraction ($1 - E$) of arterial water flows to the venous side of the capillary bed without exchanging with tissue water. Also represented in the model is the exchange of tissue water with tissue macromolecules. Adapted from (*31*).

The purpose of this article is to describe the current state of the art in CBF-based fMRI techniques and review the current understanding of the relationship between BOLD and CBF signal changes occurring during functional brain activation.

ASL TECHNIQUES

Basic Model of ASL

The theoretical modeling of MR measurements of perfusion with ASL has been extensively described (*2, 5, 25, 21–23*) and reviewed in great detail (*24–26*). Therefore, only a general description is offered here.

Figure 1 shows a schematic representation of a

typical fraction of tissue and its associated vasculature for the purposes of establishing the arterial spin-labeling model. Blood flowing through the arterial vessels with a CBF flow rate (mL g^{-1} min^{-1}) reaches the capillary bed, where a fraction E of water exchanges with tissue water in the extravascular (EV) space. The remaining fraction $(1 - E)$ of arterial water flows to the venous side of the capillary bed without exchanging with tissue water. Also represented in the model is the exchange of tissue water with tissue macromolecules. According to this model, the Bloch equations for the longitudinal magnetization of brain tissue water and macromolecular spins can be written as

$$\frac{dM_t(t)}{dt} = \frac{M_t^0 - M_t(t)}{T_{1t}} - k_{for}M_t(t) + k_{rev}M_m(t) + \text{CBF}[M_a(t) - M_v(t)]$$

$$\times \frac{dM_m(t)}{dt} = \frac{M_m^0 - M_m(t)}{T_{1m}} + k_{for}M_t(t) - k_{rev}M_m(t) \quad [1]$$

where $M_t(t)$ and $M_m(t)$ are the tissue and macromolecular magnetization per gram of brain tissue, respectively; $M_a(t)$ and $M_v(t)$ are the arterial and venous water magnetization per milliliter of arterial and venous blood, respectively; T_{1t} and T_{1m} are the tissue water and macromolecular longitudinal relaxation time constants, respectively (s); λ is the tissue/blood partition coefficient for water; E is the water extraction fraction; and k_{for} and k_{rev} are the magnetization transfer (MT) rate constants between tissue water and macromolecular protons, respectively (s^{-1}).

As reviewed elsewhere (*25, 26*), Eq. [1] can be solved for the CBF rate according to any of many different ASL approaches. In particular, ASL can be implemented according to two main labeling strategies: CASL or PASL.

CASL Technique

The CASL strategy consists of continuously labeling the arterial spins proximally to the brain. The continuous in-flow of labeled water leads to the development of a steady state of tissue magnetization. Labeling of arterial water can be accomplished either by a train of saturation pulses, as originally proposed by Detre et al. (*21*), or by flow-driven adiabatic fast passage, as proposed by Williams et al. (*2*). The latter method is used more because it puts the arterial water in antiphase with tissue water, producing the largest net change in tissue magnetization, and therefore maximizing CBF contrast. The state of labeled water when it exchanges with tissue is an important parameter in the quantification of CBF. The degree of labeling can be defined as

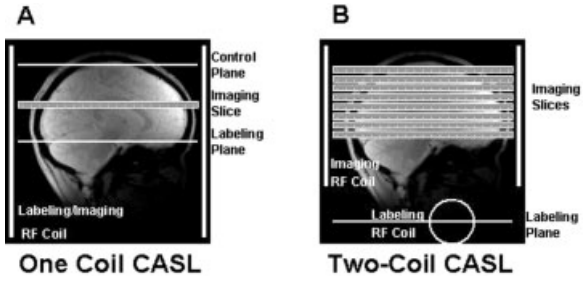

Figure 2 The RF coil arrangement for CASL experiments. (A) A single RF coil is used for labeling the arterial spins at a plane proximal to the slice of interest. In this case, off-resonance labeling of arterial blood induces magnetization transfer (MT) effects, which causes a strong decrease in tissue signal and T_1 but can be controlled for in a separate experiment where the off-resonance RF is applied in a plane located symmetrically distally from the slice of interest. (B) MT effects can be avoided with a two-coil approach, which uses a small surface coil to label the carotid arteries. This labeling coil is decoupled from the imaging coil, thus avoiding MT effects. Therefore, with the two-coil system, multislice or 3-D acquisition can be performed without subtraction artifacts and the control experiment is simply acquired without RF power applied to the labeling coil.

$$\alpha(\tau) = \alpha_0 \cdot \exp(-\tau/T_{1a})$$

$$\alpha_0 = \frac{M_a^0 - M_a}{2M_a^0} \quad [2]$$

where T_{1a} is the T_1 of arterial blood. Equation [2] shows the degree of labeling $\alpha(\tau)$ depends on the efficiency of labeling α_0 and on the transit time τ from the labeling plane to the imaging plane. The efficiency of labeling depends on the method used. For continuous saturation of arterial spins, $M_a = 0$ and $\alpha_0 = 0.5$. For continuous inversion, $\alpha_0 = 1$. The adiabatic flow-driven inversion process is very efficient, so that in practice the degree of labeling is dominated by the transit time to the imaging site. In rats, where labeling of arterial water is performed in the neck at a plane that cuts the common carotid arteries, the α value has been measured to be better than 0.8 (*6, 27*). In humans, Maccotta et al. showed an α value greater than 0.9 over a broad range of blood velocities (*28*).

CASL can be simply implemented with a single volume RF coil that covers not only the region to be imaged in the brain, but also the proximal area containing the feeding arteries. This scheme is shown in Figure 2(A). In this experiment, a labeling plane is defined to contain the main arterial supply to the

brain. For example, in rodents the labeling plane is situated in the neck, but in humans it is situated below the circle of Willis to include both the internal carotid and the vertebral arteries. The off-resonance RF radiation used to label the arterial spins also saturates tissue macromolecules, which causes a strong decrease in tissue signal and T_1 because of MT effects. Fortunately, MT effects are highly symmetric in frequency, so that an easy control can be achieved if the same off-resonance RF radiation is applied to a plane placed distally from the imaging site at an equal distance with respect to the labeling plane [Fig. 2(A)]. The solution of the Bloch equations (Eq. [1]) when tissue macromolecules are saturated [$M_m(t) = 0$] is given by

$$M_t(t) = T_{1app} \cdot M_t^0 \left\{ \frac{1}{T_{1app}} - \left[k_{for} + 2\alpha \frac{CBF}{\lambda} E \right] \times (1 - \exp(-t/T_{1app})) \right\}$$

$$\frac{1}{T_{1app}} = \frac{1}{T_{1t}} + k_{for} + \frac{CBF}{\lambda} E \qquad [3]$$

Equation [3] shows the reduction in tissue magnetization at steady state, together with the reduction in tissue T_1 to a shorter apparent constant T_{1app}, which is due to saturation of tissue macromolecules. For example, at 4.7 T the tissue signal is reduced by 75% from its equilibrium value and $T_{1app} = 0.45$ s, compared to $T_{1t} = 1.7$ s (*22*). CBF can be measured from two MR images, one in which RF is applied to the control plane and another in which RF is applied to the labeling plane:

$$CBF = \frac{\lambda}{E} \frac{1}{T_{1t}} \left[\frac{M_t^c - M_t^l}{M_t^l + (2\alpha - 1) M_t^c} \right] \qquad [4]$$

where M_t^c and M_t^l are the tissue magnetization in the control and labeled states, respectively.

As mentioned above, the one-coil implementation of CASL inconveniently saturates tissue macromolecules, causing a reduction in both in the signal amplitude an the T_1, effectively reducing the signal to noise ratio (SNR) of the CBF measurement. Furthermore, the control plane illustrated in Figure 2(A) works only for a single slice parallel to the labeling plane. Clever approaches to allow multislice imaging have been proposed (*8, 29*), but they do not avoid saturation of tissue macromolecules and therefore still suffer from poor SNR. A hardware approach to eliminate saturation of tissue macromolecules has been proposed (*6, 23*) and implemented for imaging of the rat (*6, 30–34*) and humans (*35*). The schematics of the two-coil system is shown in Figure 2(B). A small surface coil is placed over the neck region to label the carotid arteries. Because the RF field generated by the small labeling coil does not reach the brain, tissue macromolecules are not saturated, eliminating the reduction in signal intensity and shortening of T_1 due to MT effects. In addition, multislice or 3-dimensional (3-D) acquisition can be performed without subtraction artifacts. Using the two-coil system, CBF can be calculated from two images acquired with and without labeling of the arterial spins as (*23, 31*)

$$CBF = \frac{\lambda}{E} \left(\frac{1}{T_{1t}} + \delta \right) \frac{M_t^0 - M_t^l}{M_t^l + (2\alpha - 1) M_t^0}$$

$$\delta = \frac{k_{for}}{1 + k_{rev} T_{1m}} \qquad [5]$$

where δ is a term that accounts for exchange between tissue water and macromolecules. This term accounts for 17% of the CBF quantification at 4.7 T (*23*).

In addition to allowing measurements of CBF with higher SNR and more extensive coverage than the one-coil implementation of CASL, the two-coil approach had a key role in understanding the basic principles of water exchange in the brain (*30, 31*). Further, the use of a separate labeling coil significantly reduces RF power deposition, which is a critical consideration for use of CASL in humans (*35*). Unfortunately, however, the human anatomy forces placement of the labeling coil too far upstream from the region of interest in the brain, causing a significant attenuation of the degree of labeling due to transit-time decay.

PASL Approach

The pulsed approach to ASL consists of labeling a thick slab of blood upstream from the region of interest with a short RF pulse and waiting a certain time to allow the labeled blood to mix with tissue prior to acquiring the image. This idea has been implemented in a number of different ways (*3–5, 36*). The approach used by Kim (*5*) was named flow-sensitive alternating inversion recovery (FAIR), which is illustrated in Figure 3. In FAIR, the labeled image is acquired inside a slice-selective inversion slab. The uninverted blood that flows from outside the inversion slab into the inversion slab creates the desired CBF contrast, because uninverted arterial water speeds up the longitudinal relaxation of tissue water upon mixing due

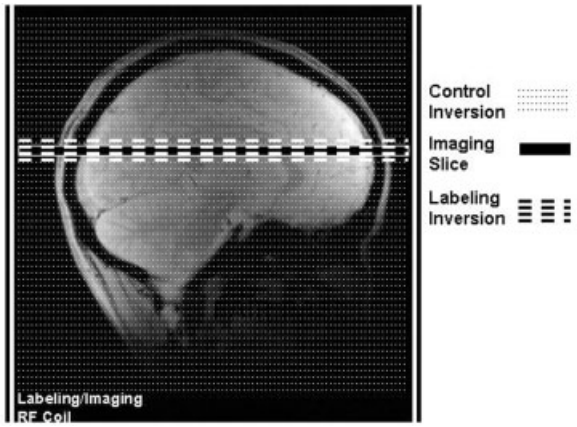

Figure 3 A scheme for FAIR pulsed arterial spin labeling (PASL). The labeled image is acquired inside a slice-selective inversion slab. The uninverted blood that flows from outside the inversion slab into the inversion slab creates the desired CBF contrast, because uninverted arterial water speeds up the longitudinal relaxation of tissue water upon mixing that is due to perfusion. The control situation is acquired after a nonselective inversion pulse, when both arterial water and tissue are inverted.

to perfusion. The control situation is acquired after a nonselective inversion pulse, when both arterial water and tissue are inverted, so that tissue relaxes back to equilibrium with the normal relaxation constant T_{1t}. Using FAIR the CBF can be quantified according to (*25, 37, 38*)

$$\mathrm{CBF} = \frac{\lambda}{2\alpha_0}\frac{\Delta M_t}{M_t^0}\left[\frac{1/T_{1a} - 1/T_{1app}}{\exp(-\mathrm{TI}/T_{1app}) - \exp(-\mathrm{TI}/T_{1a})}\right] \quad [6]$$

where ΔM_t is the signal difference between the control and labeled images, TI is the inversion time, and T_{1a} is the T_1 of arterial blood. Multislice acquisition can also be performed with FAIR (*1*). In this case the slice-selective inversion slab must contain all imaging slices, and the different transit time to different slices could compromise quantification of CBF. However, it has been reported that when relative CBF changes are determined in multislice FAIR experiments, errors induced by different transit times are not significant (*39*). Relative CBF changes measured by PASL are in very good agreement with those measured by $H_2^{15}O$ positron emission tomography (PET) in the same region and subject during the identical stimulation task (*39*). Thus, FAIR is also an excellent perfusion technique for the measurement of relative CBF changes induced by neural activity or other external perturbations.

CURRENT APPLICATIONS OF CBF-BASED fMRI

The coupling between neural activity and CBF makes ASL-based MRI techniques excellent tools for monitoring brain function in both normal and pathological states. Many pathophysiological disorders of the brain are associated with alterations in normal perfusion values, which can be mapped and quantified or followed in time with ASL techniques. In particular, ASL has the potential advantages of BOLD because it can quantify resting CBF, as well as CBF changes, making results useful in longitudinal studies or in comparisons among clinical populations. The applications of ASL-based techniques in assessing brain disorders are currently quite broad and beyond the scope of this article. The reader is referred to other reviews (*40–42*) of current clinical applications of ASL.

The CBF changes induced by external perturbations will be, in theory, the same whether measurements are performed on high or low field systems. Therefore, relative CBF measurements using the perfusion-based fMRI technique can be performed even at low magnetic fields, provided adequate SNR can be achieved, although high fields provide a higher SNR and a longer T_1 of water.

The BOLD signal is sensitive to a large static susceptibility effect around the tissue to sinus boundaries, making it difficult to obtain high quality images in the frontal and temporal areas. Thus, it is difficult to obtain fMRI in these areas. Because the perfusion-based technique does not rely on the susceptibility effect for its contrast, a spin–echo (SE) data collection scheme can be used for recovering signals in high susceptibility regions. Hence, perfusion-based fMRI is better than the conventional BOLD method for mapping highly susceptible areas.

In the functional MRI studies, baseline drift is a problem because functional maps are calculated from a comparison between control and task-induced signal intensities. This drift may be due to physiological changes induced by effects such as anxiety and anticipation, the subject's motion (even if subpixel movements), system instabilities due to changes in eddy current compensation and field drift, a change in gain setting at different scanning sessions, and an approach to steady-state magnetization if relatively fast repetition of RF pulses is employed. Slight, not abrupt, baseline changes can be corrected by subtraction of an image from its neighbor image (*5*), improving the sensitivity of perfusion-based fMRI. Also, this property of perfusion-based fMRI can allow the use of

perfusion-based fMRI for longitudinal studies. For intersubject or intersession intrasubject comparisons, the perfusion-based techniques are the method of choice.

Most of the fMRI studies performed today are based on the BOLD contrast, because of its high contrast to noise ratio (CNR) and simplicity of implementation. However, the BOLD contrast mechanism depends on a complex interplay between CBF, CBV, and $CMRO_2$ (*17, 18*). The intrinsic relationship between these variables is not fully understood. Positive BOLD signal changes are presumably caused by increases in CBF that are unmatched by the corresponding increases in $CMRO_2$ (*17, 19*). On the other hand, negative BOLD signals can be generated by early increases in $CMRO_2$ prior to increases in CBF or by increases in CBV. Therefore, to better understand the physiological mechanisms underlying functional hemodynamic changes, it is fundamental to obtain simultaneous measurements of BOLD, CBF, and CBV changes. For the remainder of this article, we focus on simultaneous measurements of BOLD and CBF performed in animals and humans and attempt to provide a current understanding of hemodynamic regulation during functional brain activation.

Spatial Specificity

Animal studies comparing BOLD and CBF regions of activation using fMRI have been recently reported in the rat somatosensory cortex (*33, 34, 43, 44*) and in the cat visual cortex (*45*). These animal studies, performed at high magnetic field strength, have established important considerations regarding the spatial localization of BOLD with respect to CBF and to the expected site of increased electrical activity. For example, Figure 4(A) shows typical BOLD and CBF cross-correlation functional maps obtained at 9.4 T during forepaw stimulation in a rat. Good agreement in the spatial location of activation regions was observed, and the mean separation between the center of the BOLD and the CBF active regions was determined to be less than one pixel (*33*). In addition, the number of pixels in the BOLD region was strongly correlated to the number of pixels in the CBF region. Figure 4(B) shows a comparison of the overlap of BOLD, CBF, and calcium influx, as probed by T_1 weighted images sensitive to the calcium analog Mn^{++} (*43*). The highest CBF and calcium influx change was located in layer 4 of the somatosensory cortex. It demonstrates the excellent overlap between the regions of activation as reported by BOLD, CBF, and Mn-dependent T_1 contrast, which is proof of the excellent spatial localization of BOLD signal changes

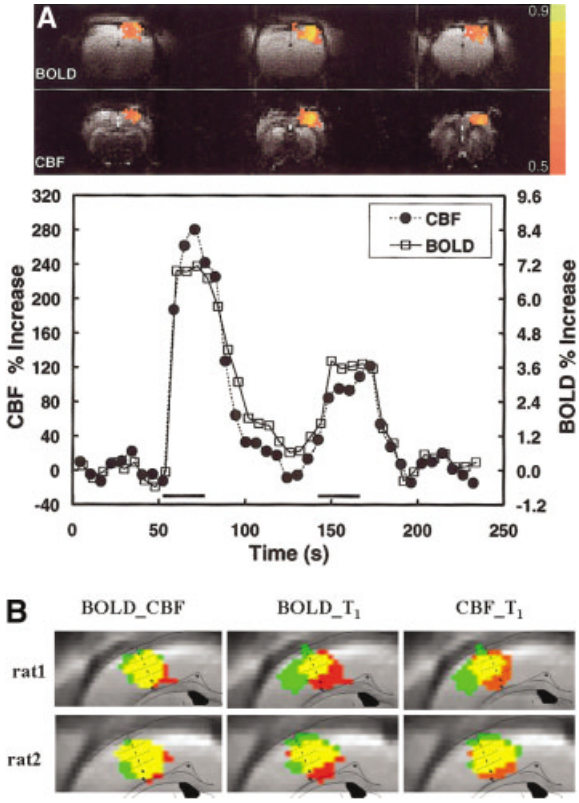

Figure 4 (A) BOLD (top row) and CBF (bottom row) activation maps of the rat brain upon electrical stimulation of the right forepaw. The bottom graph shows the time course of a 9 pixel ROI placed on the center of the active areas (middle slice) of the BOLD and CBF maps. The temporal correlation coefficient between the BOLD and the CBF time courses was 0.92. (B) Spatial overlap of hemodynamic versus calcium-dependent activity. The first column shows the combined maps of BOLD (red), CBF (green), and the overlap between the two (yellow). The second column shows the combined maps of BOLD (red), T_1 (green), and the overlap between the two maps (yellow). The third column shows the combined maps of CBF (red), T_1 (green), and the overlap between the two (yellow).

at high magnetic field strengths. However, although CBF maintains its high spatial specificity at all magnetic field strengths, the same cannot be said of the BOLD contrast. The functional CBF maps measured with FAIR in response to single orientation stimulation of the cat visual cortex at 4.7 T were specific to a submillimeter columnar structure, in contrast to gradient–echo (GE) BOLD, which could not resolve columnar structures (*45*). This indicates that perfusion-based fMRI provides higher spatial specificity than BOLD fMRI at medium and low magnetic fields such as 4.7 T.

CBF and BOLD studies were also performed in humans during finger movements and visual stimula-

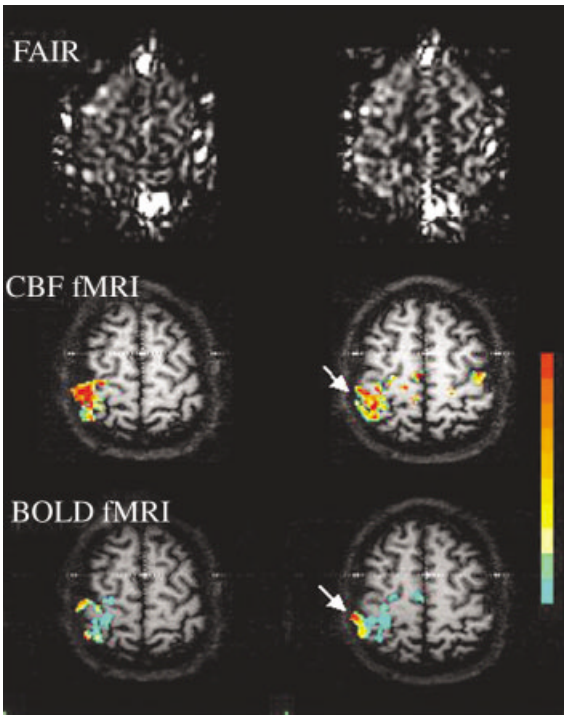

Figure 5 Multislice FAIR measurements of a normal volunteer during finger movement at 4 T. The panels show FAIR contrast (top), CBF-weighted fMRI maps overlaid on anatomic images (middle), and BOLD fMRI maps (bottom). CBF-weighted fMRI was obtained using the FAIR technique, while BOLD maps were obtained from nonslice selective inversion-recovery images acquired as part of FAIR. The color bar shows from 10 to >90% changes for CBF and from 1 to >9% changes for BOLD. The arrows indicate the central sulcus. It is interesting that the CBF-weighted fMRI signals localize to tissue areas, not to large vessels. Thus, higher spatial specificity can be obtained using CBF techniques. Adapted from (*1*).

tion at 4 T (*1, 37, 46, 47*). Generally, supramillimeter activation sites were consistent between CBF and GE BOLD fMRI maps and stimulation frequency-dependent activation covaried in both functional images. However, as shown in Figure 5, GE BOLD maps show "activation" in large draining veins, such as the Rolendic vein in the central sulcus, which are absent in FAIR-based fMRI.

In addition to being strongly related to the strength of the magnetic field, BOLD is also very sensitive to the type of MRI pulse sequence used (*44, 45, 48–51*). Inspecting the vascular contribution to BOLD fMRI signals constitutes a fundamental step toward a better understanding of the spatial specificity issues in BOLD. In particular, the BOLD effect is sensitive to the venous blood volume and vessel size and orientation (*17, 18, 52*). To comprehend the nature of the vascular contribution, it is important to separate the macrovascular from the microvascular components (*53*). The microvascular or tissue component is defined as coming from capillaries and surrounding tissues, whereas the macrovascular component arises from large venules and veins. The microvascular effect is believed to be close to the site of neuronal activity. However, unlike capillaries, there is not a high density of large blood vessels in the brain; thus, functional maps based on the macrovasculature can be significantly distant from the actual site of neural activity. Therefore, it is desirable to minimize the macrovascular contribution. According to the BOLD model (*18, 52*), vascular contributions to the BOLD signal are composed of EV and intravascular (IV) effects. The EV contribution from large vessels is linearly dependent on the magnetic field strength (B_0), whereas the EV contribution from microvessels increases quadratically with B_0. This suggests that high magnetic fields can increase the relative contribution of the microvascular component to the BOLD signal. The EV component of microvessels contributes to both SE and GE fMRI as a result of dynamic signal averaging induced by water diffusion during an echo time (TE). However, the EV component of large

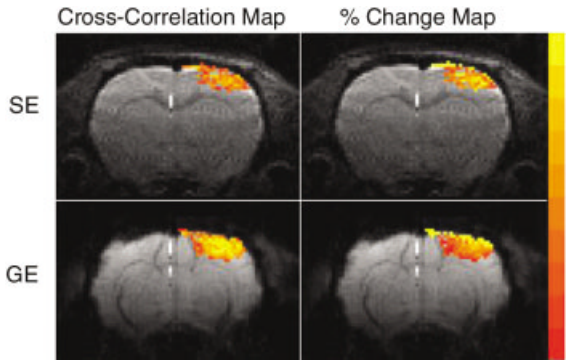

Figure 6 A comparison between spin–echo (top) and gradient–echo (bottom) BOLD fMRI. The BOLD statistical maps are overlaid on two-segment EPI images acquired at 9.4 T at TE = 16 ms (GE) or 40 ms (SE). The SE and GE images are diffusion weighted (b = 100 s/mm^2 for SE, 200 s/mm^2 for GE). On the left, the CCC maps are color coded between 0.5 and 0.9, while the relative BOLD signal change maps shown on the right are color coded between 3 and 11% signal changes. The functional maps on the left present high cross-correlation coefficient (CCC) values in the deep layers of the somatosensory cortex for both SE and GE images. The SE BOLD percentage of increase map (top right) agrees with the corresponding CCC map (top left). However, the GE BOLD percentage of signal increase map (bottom right) presents its highest signal increases at the pial surface, where large superficial veins are located. Adapted from (*50*).

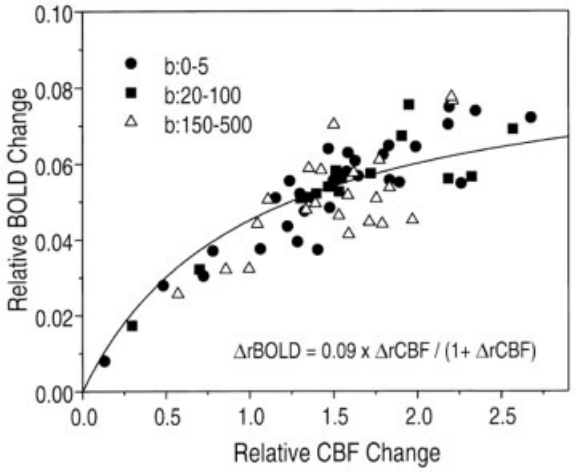

Figure 7 A comparison of the relative SE BOLD and CBF signal changes during electrical stimulation of the rat forepaw. Data are grouped into three diffusion-weighting ranges. There is no difference in the correlation between SE BOLD and CBF at different diffusion weightings. The solid curve shows the fit of the data to the function indicated on the graph. Adapted from (*44*).

vessels contributes only to GE fMRI, not to SE fMRI, because the 180° RF pulse in SE fMRI can refocus the dephasing effect of static field inhomogeneities around large vessels (*18, 52, 54, 55*). Applying flow-sensitive bipolar gradients cannot reduce these EV effects. The vascular contribution to BOLD was extensively studied at 9.4 T. In one study, GE and SE BOLD contrast was compared in the presence of graded diffusion weighting to reveal the contribution from large vessels to BOLD (*50*). Figure 6 shows a comparison between diffusion-weighted GE and SE BOLD fMRI in a rat model of somatosensory stimulation. The SE image was acquired using $b = 100$ s/mm^2, and the GE image was acquired at $b = 200$ s/mm^2. Whereas the SE image shows the largest signal changes in the middle layers of the somatosensory cortex, the GE image presents high signal increases at the pial surface, where large superficial veins are located. A combination of a long TE and diffusion weighting helps minimize the IV component of both the GE and SE images. However, in GE fMRI, the highest percentage of signal changes still take place near the edge of the brain, because the EV component from large vessels cannot be suppressed by a GE sequence, even in the presence of diffusion-sensitizing gradients (*50*). Another study compared SE BOLD to CBF in the same rat model, leading to the conclusion that both CBF- and SE BOLD-based fMRI yield tissue-specific maps at high magnetic fields (*44*). To obtain accurate high-resolution functional maps, it is crucial to remove large vessel contributions. It is important to mention that SE BOLD at 1.5 T contains predominantly an IV component (*56, 57*). Therefore, the combination of high magnetic fields with diffusion-weighted SE sequences that are insensitive to draining veins constitutes the best approach to BOLD-based fMRI at submillimeter resolution.

Magnitude of Signal Changes

CBF-based fMRI can provide better localized mapping of neuronal activation because it is not sensitive to large draining vessels. The CBF contrast mostly reflects truly perfusing spins that have permeated the capillary walls and entered the EV space. Because relative CBF changes are linearly correlated to metabolic changes (*19, 58*), CBF can play the role of a gold standard for quantifying neuronal activity. The quantification of absolute CBF values requires suppression of large vessel artifacts, in particular those originating from large arteries. We have observed a 10–20% reduction in resting CBF values with the use of small ($b = 20$–500 s/mm^2) diffusion-sensitizing gradients (*30, 44*). However, the use of diffusion-sensitizing gradients has no effect of quantifying relative CBF changes during somatosensory stimulation in rats (*44*), suggesting the arterial vasodilatation is proportional to the CBF changes. This is consistent with our previous finding of significant arterial CBV changes during increased CBF (*51*). Taken together, the contribution of large vessels to functional CBF changes, as measured by the CASL technique, does not alter tissue-level relative CBF changes.

Because the BOLD contrast is dependent on various physiological and anatomical parameters, it is important to compare BOLD signal changes with CBF-based fMRI. Relative CBF and BOLD signal changes during somatosensory stimulation in rats have been extensively compared at 9.4 T (*33, 34, 43, 44*). Figure 7 shows an equivalent plot of SE BOLD versus CBF changes. Individual diffusion-sensitized fMRI data obtained from 10 animals (12 paws) are plotted; low ($b = 0$–5 s/mm^2), intermediate ($b = 20$–100 s/mm^2), and high ($b = 150$–500 s/mm^2) diffusion gradient data are shown. The relationship between relative BOLD and CBF changes was identical in all groups, indicating that the presence of diffusion-weighting gradients did not affect any signal. This is consistent with previous observations that the SE BOLD contrast has its origin in EV dynamic averaging effects around small vessels (*50*), and therefore our results show excellent correlation between SE BOLD and CBF changes during functional stimulation at high spatial resolution. When the large

vascular component is suppressed, CBF and BOLD fMRI contrasts are closely coupled and originate from a similar anatomical location within a single voxel. However, the relationship between BOLD and CBF changes is highly nonlinear, especially at high CBF changes. Such a relationship can also be found in CBF and GE BOLD signals obtained from a large region of interest, but not on a pixel by pixel basis (*47*). This consideration should be taken into account when trying to use BOLD-based fMRI as a quantitative method for mapping neuronal activity.

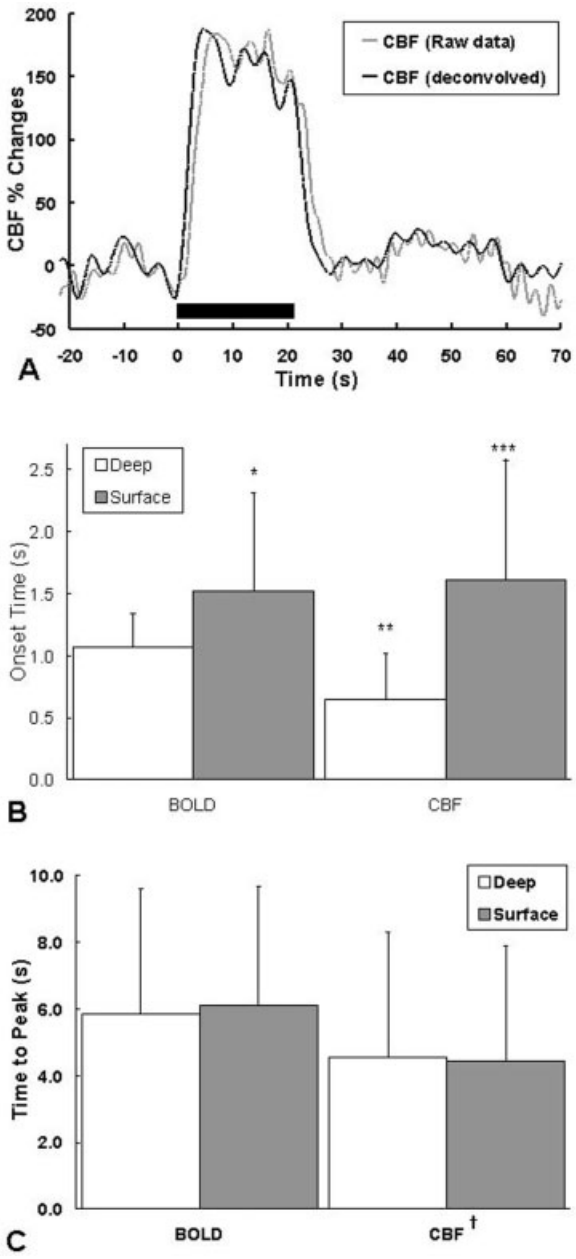

Temporal Characteristics

The inherent temporal resolution of ASL methods of quantifying CBF is inherently low. Proper perfusion contrast is achieved when enough time is allowed for the labeled spins to travel into the region of interest and exchange with tissue spins. In addition, it is necessary to acquire two images, usually in an interleaved manner, to determine CBF: one with spin labeling and another as a control. Thus, the typical temporal resolution of ASL methods is on the order of a few seconds (3.5, 5.8, and 8). In order to obtain dynamic CBF changes with high temporal and spatial resolution, we have recently devised a novel MRI technique, coined pseudocontinuous ASL (PCASL) (*32*). The PCASL technique consists of using a short ASL RF pulse in conjunction with an ultrafast imaging sequence, such as echo–planar or spiral imaging. The ASL RF pulse is made short to allow for high temporal resolution but long compared to the imaging time, so that high labeling duty cycles (and thus the efficiency) can be maintained. For example, PCASL has been implemented using 78-ms ASL pulses in conjunction with a 30-ms echo-planar imaging (EPI) sequence (*32, 24*). Under these conditions, CBF images could be formed every 108 ms with a labeling efficiency of 59% ($\alpha = 0.59$). Two separate experiments are performed in PCASL: one with spin labeling and the other as a control. Once the CBF images are formed according to Eq. [5], an analysis of the temporal characteristics of the CBF time course is desired. For this, a temporal deconvolution of the CBF time course becomes necessary. This is because instantaneous changes in CBF cause slow variations in the MRI signal. The basic principle of the ASL technique is the transfer of the longitudinal magneti-

Figure 8 (A) MRI-measured (gray) and true (black) CBF curves obtained at 108-ms temporal resolution during electrical stimulation of the rat forepaw. The MRI-measure curve was deconvolved with the tissue T_1 decay curve to produce the true CBF response. (B) Averaged onset times of CBF and BOLD in the surface (gray bars) and deep (white bars) regions of the somatosensory cortex. (*) The onset of the BOLD response in the cortical surface was significantly longer than deep in the cortex ($p < 0.03$). (**) CBF changes in the deep cortex occurred earlier than the corresponding BOLD changes ($p < 0.003$). (***) The onset of superficial CBF changes was significantly delayed with respect to deep in the cortex ($p < 0.004$). (C) Averaged times to peak of CBF and BOLD. There was no significant time to peak differences across regions for either BOLD ($p > 0.28$) or CBF ($p > 0.39$). (*) However, the CBF peak response occurred faster than the BOLD response in both regions ($p < 0.001$). Error bars = 1 SD. Adapted from (*34*).

zation state of the arterial water spins to the tissue spins. This transfer is limited by T_{1app}, repetition time (TR), and the RF flip angle θ and cannot occur instantly. Therefore, step changes in perfusion (and, consequently, in T_{1app}) are only reflected a few seconds later in the tissue magnetization. By performing a deconvolution of the MRI-measured CBF signal with the initial magnetization decay curve, this latency in the MRI measured CBF response can be removed. After this deconvolution process, the resulting CBF time course accurately reflects the dynamics of the actual CBF changes.

Figure 8(A) shows the MRI-estimated (gray) and the deconvolved CBF (black) time courses obtained during somatosensory stimulation in rats using the PCASL technique. The MRI-estimated CBF curve was deconvolved with the initial 10 s of the control magnetization decay, generating the deconvolved CBF signal. It can be clearly seen how the CBF response measured with MRI is delayed with respect to the deconvolved curve. Note from Figure 8(A) that the deconvolution adds oscillatory noise to the resulting curve. However, the CBF changes elicited by this model of activation are very robust, to the point that the results presented here are not compromised by the additional noise introduced by the deconvolution process. Because we used GE EPI as the readout imaging sequence in our PCASL technique, BOLD signal changes could be measured from the control series of images and directly compared to the corresponding CBF changes. Figure 8(B) shows the onset time of BOLD and CBF in the superficial and deep regions of the somatosensory cortex following the onset of stimulation. CBF changes in the deep layers of the somatosensory cortex occurred earlier than the corresponding BOLD changes ($p < 0.003$). However, in the superficial layers, the onset of the CBF response was delayed and it was similar to the latency of the superficial BOLD signal changes. Figure 8(C) shows the BOLD and CBF times to peak. The CBF peak response occurred faster than the BOLD response in both regions ($p < 0.001$).

CONCLUSIONS

Perfusion-based fMRI is specific to tissue signal changes, a critical feature for proper quantification of the functional response and for high-resolution functional mapping. Unlike the conventional BOLD technique, the CBF change is an excellent index of the magnitude of neural activity change. Perfusion-based fMRI provides high spatial resolution because the contribution of draining veins to the CBF-weighted signal is minimal. The perfusion changes induced by neural activity are faster than the BOLD response. By combining ASL with the BOLD technique, both the CBF and venous oxygenation level can be obtained, which can be used for examining the sources of the BOLD contrast. Because slow baseline changes can be eliminated by pairwise subtraction of images, CBF-based functional images can be obtained even when baseline signals are modulated because of system instabilities, different gain settings, or physiological changes. Thus, perfusion-based fMRI is the tool of choice for longitudinal functional imaging studies. Overall, the perfusion-based fMRI technique is an excellent complementary approach for functional mapping of human and animal brains.

ACKNOWLEDGMENTS

The authors would like to acknowledge the financial support from the National Institutes of Health (to the University of Minnesota) and the Keck Foundation.

REFERENCES

1. Kim SG, Tsekos NV, Ashe J. Multi-slice perfusion-based functional MRI using the FAIR technique: Comparison of CBF and BOLD effects. NMR Biomed 1997; 10:191–196.
2. Williams DS, Detre JA, Leigh JS, Koretsky AP. Magnetic resonance imaging of perfusion using spin inversion of arterial water. Proc Natl Acad Sci USA 1992; 89:212–216.
3. Kwong KK, Belliveau JW, Chesler DA, Goldberg IE, Weisskoff RM, Poncelet BP, Kennedy DN, Hoppel BE, Cohen MS, Turner R. Dynamic magnetic resonance imaging of human brain activity during primary sensory stimulation. Proc Natl Acad Sci USA 1992; 89:5675–5679.
4. Edelman RR, Siewert B, Darby DG, Thangaraj V, Nobre AC, Mesulam MM, Warach S. Qualitative mapping of cerebral blood flow and functional localization with echo–planar MR imaging and signal targeting with alternating radio frequency. Radiology 1994; 192:513–520.
5. Kim SG. Quantification of relative cerebral blood flow change by flow-sensitive alternating inversion recovery (FAIR) technique: Application to functional mapping. Magn Reson Med 1995; 34:293–301.
6. Silva AC, Zhang W, Williams DS, Koretsky AP. Multi-slice MRI of rat brain perfusion during amphetamine stimulation using arterial spin labeling. Magn Reson Med 1995; 33:209–214.
7. Wong EC, Buxton RB, Frank LR. Implementation of quantitative perfusion imaging techniques for func-

tional brain mapping using pulsed arterial spin labeling. NMR Biomed 1997; 10:237–249.
8. Alsop DC, Detre JA. Multisection cerebral blood flow MR imaging with continuous arterial spin labeling. Radiology 1998; 208:410–416.
9. Dixon WT, Du LN, Faul DD, Gado MH, Rossnick S. Projection angiograms of blood labeled by adiabatic fast passage. Magn Reson Med 1986; 3:454–462.
10. Roy CS, Sherrington CS. On the regulation of the blood supply of the brain. J Physiol 1890; 11:85–108.
11. Raichle ME. Behind the scenes of functional brain imaging: A historical and physiological perspective. Proc Natl Acad Sci USA 1998; 95:765–772.
12. Bandettini PA, Wong EC, Hinks RS, Tikofsky RS, Hyde JS. Time course EPI of human brain function during task activation. Magn Reson Med 1992; 25: 390–397.
13. Ogawa S, Tank DW, Menon RS, Ellermann JM, Kim S-G, Merkle H, Ugurbil K. Intrinsic signal changes accompanying sensory stimulation: Functional brain mapping with magnetic resonance imaging. Proc Natl Acad Sci USA 1992; 89:5951–5955.
14. Turner R. Magnetic resonance imaging of brain function. Am J Physiol Imaging 1992; 7(3–4):136–145.
15. Kwong KK, Chesler DA, Weisskoff RM, Donahue KM, Davis TL, Ostergaard L, Campbell TA, Rosen BR. MR perfusion studies with T1-weighted echo planar imaging. Magn Reson Med 1995; 34:878–887.
16. Belliveau JW, Rosen BR, Kantor HL, Rzedzian RR, Kennedy DN Jr, McKinstry RC, Vevea JM, Cohen MS, Pykett IL, Brady TJ. Functional cerebral imaging by susceptibility-contrast NMR. Magn Reson Med 1990; 14:538–546.
17. Ogawa S, Menon RS, Tank DW, Kim SG, Merkle H, Ellermann JM, Ugurbil K. Functional brain mapping by blood oxygenation level-dependent contrast magnetic resonance imaging. A comparison of signal characteristics with a biophysical model. Biophys J 1993; 64: 803–812.
18. Weisskoff RM, Zuo CS, Boxerman JL, Rosen BR. Microscopic susceptibility variation and transverse relaxation: Theory and experiment. Magn Reson Med 1994; 31:601–610.
19. Fox PT, Raichle ME. Focal physiological uncoupling of cerebral blood flow and oxidative metabolism during somatosensory stimulation in human subjects. Proc Natl Acad Sci USA 1986; 83:1140–1144.
20. Roland PE, Eriksson L, Stone-Elander S, Widen L. Does mental activity change the oxidative metabolism of the brain? J Neurosci 1987; 7:2373–2389.
21. Detre JA, Leigh JS Jr, Williams DS, Koretsky AP. Perfusion imaging. Magn Reson Med 1992; 23:37–45.
22. Zhang W, Williams DS, Detre JA, Koretsky AP. Measurement of brain perfusion by volume-localized NMR spectroscopy using inversion of arterial water spins: Accounting for transit time and cross-relaxation. Magn Reson Med 1992; 25:362–371.
23. Zhang W, Silva AC, Williams DS, Koretsky AP. NMR measurement of perfusion using arterial spin labeling without saturation of macromolecular spins. Magn Reson Med 1995; 33:370–376.
24. Detre JA, Zhang W, Roberts DA, Silva AC, Williams DS, Grandis DJ, Koretsky AP, Leigh JS. Tissue specific perfusion imaging using arterial spin labeling. NMR Biomed 1994; 7:75–82.
25. Calamante F, Thomas DL, Pell GS, Wiersma J, Turner R. Measuring cerebral blood flow using magnetic resonance imaging techniques. J Cereb Blood Flow Metab 1999; 19:701–735.
26. Barbier EL, Lamalle L, Decorps M. Methodology of brain perfusion imaging. J Magn Reson Imaging 2001; 13:496–520.
27. Zhang W, Williams DS, Koretsky AP. Measurement of rat brain perfusion by NMR using spin labeling of arterial water: In vivo determination of the degree of spin labeling. Magn Reson Med 1993; 29:416–421.
28. Maccotta L, Detre JA, Alsop DC. The efficiency of adiabatic inversion for perfusion imaging by arterial spin labeling. NMR Biomed 1997; 10:216–221.
29. Talagala SL, Barbier EL, Williams DS, Silva AC, Koretsky AP. Multi-slice perfusion MRI using continuous arterial water labeling controlling for MT effects with simultaneous proximal and distal RF irradiation. In Proceedings of the 6th Annual Meeting of the ISMRM, Sydney, Australia, 1998; Vol. 1, p 381–381.
30. Silva AC, Williams DS, Koretsky AP. Evidence for the exchange of arterial spin-labeled water with tissue water in rat brain from diffusion-sensitized measurements of perfusion. Magn Reson Med 1997; 38:232–237.
31. Silva AC, Zhang W, Williams DS, Koretsky AP. Estimation of water extraction fractions in rat brain using magnetic resonance measurement of perfusion with arterial spin labeling. Magn Reson Med 1997; 37:58–68.
32. Silva AC, Kim SG. Pseudo-continuous arterial spin labeling technique for measuring CBF dynamics with high temporal resolution. Magn Reson Med 1999; 42: 425–429.
33. Silva AC, Lee SP, Yang G, Iadecola C, Kim SG. Simultaneous blood oxygenation level-dependent and cerebral blood flow functional magnetic resonance imaging during forepaw stimulation in the rat. J Cerebr Blood Flow Metab 1999; 19:871–879.
34. Silva AC, Lee SP, Iadecola C, Kim SG. Early temporal characteristics of cerebral blood flow and deoxyhemoglobin changes during somatosensory stimulation. J Cerebr Blood Flow Metab 2000; 20:201–206.
35. Zaharchuk G, Ledden PJ, Kwong KK, Reese TG, Rosen BR, Wald LL. Multislice perfusion and perfusion territory imaging in humans with separate label and image coils. Magn Reson Med 1999; 41:1093–1098.
36. Wong EC, Buxton RB, Frank LR. Quantitative imaging of perfusion using a single subtraction (QUIPSS and QUIPSS II). Magn Reson Med 1998; 39:702–708.
37. Kim SG, Tsekos NV. Perfusion imaging by a flow-sensitive alternating inversion recovery (FAIR) tech-

nique: Application to functional brain imaging. Magn Reson Med 1997; 37:425–435.
38. Tsekos NV, Zhang F, Merkle H, Nagayama M, Iadecola C, Kim SG. Quantitative measurements of cerebral blood flow in rats using the FAIR technique: Correlation with previous iodoantipyrine autoradiographic studies. Magn Reson Med 1998; 39:564–573.
39. Zaini MR, Strother SC, Anderson JR, Liow JS, Kjems U, Tegeler C, Kim SG. Comparison of matched BOLD and FAIR 4.0T-fMRI with [15O]water PET brain volumes. Med Phys 1999; 26:1559–1567.
40. Detre JA, Floyd TF. Functional MRI and its applications to the clinical neurosciences. Neuroscientist 2001; 7:64–79.
41. Warach S. Use of diffusion and perfusion magnetic resonance imaging as a tool in acute stroke clinical trials. Curr Control Trials Cardiovasc Med 2001; 2:38–44.
42. Detre JA, Wang J. Technical aspects and utility of fMRI using BOLD and ASL. Clin Neurophysiol 2002; 113:621–634.
43. Duong TQ, Silva AC, Lee SP, Kim SG. Functional MRI of calcium-dependent synaptic activity: Cross correlation with CBF and BOLD measurements. Magn Reson Med 2000; 43:383–392.
44. Lee SP, Silva AC, Kim SG. Comparison of diffusion-weighted high-resolution CBF and spin–echo BOLD fMRI at 9.4 T. Magn Reson Med 2002; 47:736–741.
45. Duong TQ, Kim DS, Ugurbil K, Kim SG. Localized cerebral blood flow response at submillimeter columnar resolution. Proc Natl Acad Sci USA 2001; 98:10904–10909.
46. Kim SG, Ugurbil K. Comparison of blood oxygenation and cerebral blood flow effects in fMRI: Estimation of relative oxygen consumption change. Magn Reson Med 1997; 38:59–65.
47. Zhu XH, Kim SG, Andersen P, Ogawa S, Ugurbil K, Chen W. Simultaneous oxygenation and perfusion imaging study of functional activity in primary visual cortex at different visual stimulation frequency: Quantitative correlation between BOLD and CBF changes. Magn Reson Med 1998; 40:703–711.
48. Frahm J, Merboldt KD, Hanicke W, Kleinschmidt A, Boecker H. Brain or vein—Oxygenation or flow? On signal physiology in functional MRI of human brain activation. NMR Biomed 1994; 7:45–53.
49. Kim SG, Hendrich K, Hu X, Merkle H, Ugurbil K. Potential pitfalls of functional MRI using conventional gradient-recalled echo techniques. NMR Biomed 1994; 7:69–74.
50. Lee SP, Silva AC, Ugurbil K, Kim SG. Diffusion-weighted spin–echo fMRI at 9.4 T: Microvascular/tissue contribution to BOLD signal changes. Magn Reson Med 1999; 42:919–928.
51. Lee SP, Duong TQ, Yang G, Iadecola C, Kim SG. Relative changes of cerebral arterial and venous blood volumes during increased cerebral blood flow: Implications for BOLD fMRI. Magn Reson Med 2001; 45:791–800.
52. Ogawa S, Menon RS, Kim SG, Ugurbil K. On the characteristics of functional magnetic resonance imaging of the brain. Annu Rev Biophys Biomol Struct 1998; 27:447–474.
53. Song AW, Wong EC, Tan SG, Hyde JS. Diffusion weighted fMRI at 1.5 T. Magn Reson Med 1996; 35:155–158.
54. Bandettini PA, Wong EC, Jesmanowicz A, Hinks RS, Hyde JS. Spin–echo and gradient–echo EPI of human brain activation using BOLD contrast: A comparative study at 1.5 T. NMR Biomed 1994; 7:12–20.
55. van Zijl PC, Eleff SM, Ulatowski JA, Oja JM, Ulug AM, Traystman RJ, Kauppinen RA. Quantitative assessment of blood flow, blood volume and blood oxygenation effects in functional magnetic resonance imaging. Nat Med 1998; 4:159–167.
56. Zhong J, Kennan RP, Fulbright RK, Gore JC. Quantification of intravascular and extravascular contributions to BOLD effects induced by alteration in oxygenation or intravascular contrast agents. Magn Reson Med 1998; 40:526–536.
57. Oja JM, Gillen J, Kauppinen RA, Kraut M, van Zijl PC. Venous blood effects in spin–echo fMRI of human brain. Magn Reson Med 1999; 42:617–626.
58. Sokoloff L, Reivich M, Kennedy C, Des Rosiers MH, Patlak CS, Pettigrew KD, Sakurada O, Shinohara M. The [14C]deoxyglucose method for the measurement of local cerebral glucose utilization: Theory, procedure, and normal values in the conscious and anesthetized albino rat. J Neurochem 1977; 28:897–916.